REPORT DOCUMENTATION PAGE

1. REPORT DATE (DD-MM-YYYY)	2. REPORT TYPE	3. DATES COVERED (From - To)
30-11-2009	REPRINT	

4. TITLE AND SUBTITLE

A new instrument for thermal electron attachment at high temperature: NF_3 and CH_3Cl attachment rate constants up to 1100K

5a. CONTRACT NUMBER

5b. GRANT NUMBER

5c. PROGRAM ELEMENT NUMBER
61102F

6. AUTHOR(S)

Miller, T.M.*, J.F. Friedman**, J.S. Williamson*, L.C. Schaffer# and A.A. Viggiano

5d. PROJECT NUMBER
2303

5e. TASK NUMBER
HP

5f. WORK UNIT NUMBER
A1

7. PERFORMING ORGANIZATION NAME(S) AND ADDRESS(ES)

Air Force Research Laboratory
29 Randolph Road
Hanscom AFB MA 01731-3010

8. PERFORMING ORGANIZATION REPORT NUMBER

AFRL-RV-HA-TR-2009-1113

9. SPONSORING / MONITORING AGENCY NAME(S) AND ... **YM(S)**

20091207053

12. DISTRIBUTION / AVAILABILITY STATEMENT

Approved for Public Release; Distribution Unlimited

14. ABSTRACT

A new high temperature flowing afterglow Langmuir probe (HT-FALP) apparatus is described. A movable Langmuir probe and a four-needle reactant gas inlet were fitted to an existing high temperature flowing afterglow apparatus. The instrument is suitable for study of electron attachment from 300–1200 K, the upper limit set to avoid softening of the quartz flow tube. We present results for two reactions over extended ranges: NF_3 (300–900 K) and CH_3Cl (600–1100 K). Electron attachment rate constants for NF_3 had been measured earlier using our conventional FALP apparatus. Those measurements were repeated with the FALP and then extended to 900 K with the HT-FALP. CH_3Cl attaches electrons too weakly to study with the low temperature FALP but reaches a value of $\sim 10^{-9}$ cm^3 s^{-1} at 1100 K. F^- is produced in NF_3 attachment at all temperatures and Cl^- in CH_3Cl attachment, as determined by a quadrupole mass spectrometer at the end of the flow tube. Future modifications to increase the plasma density should allow study of electron-ion recombination at high temperatures. © 2009 American Institute of Physics.
[DOI: 10.1063/1.3097185]

15. SUBJECT TERM

Electron attachment   Temperature dependence   Rate constants   Methyl chloride

16. SECURITY CLASSIFICATION OF:			17. LIMITATION OF ABSTRACT	18. NUMBER OF PAGES	19a. NAME OF RESPONSIBLE PERSON A.A. Viggiano
a. REPORT UNCLAS	b. ABSTRACT UNCLAS	c. THIS PAGE UNCLAS	SAR		19b. TELEPHONE NUMBER (include area code)

DTIC COPY

A new instrument for thermal electron attachment at high temperature: NF$_3$ and CH$_3$Cl attachment rate constants up to 1100 K

Thomas M. Miller,[1,a] Jeffrey F. Friedman,[1,b] John S. Williamson,[1,a] Linda C. Schaffer,[2] and A. A. Viggiano[1,c]

[1]*Air Force Research Laboratory, Space Vehicles Directorate, 29 Randolph Road, Hanscom Air Force Base, Massachusetts 01731-3010, USA*
[2]*College of Education, University of New Mexico, Albuquerque, New Mexico 87131, USA*

A new high temperature flowing afterglow Langmuir probe (HT-FALP) apparatus is described. A movable Langmuir probe and a four-needle reactant gas inlet were fitted to an existing high temperature flowing afterglow apparatus. The instrument is suitable for study of electron attachment from 300–1200 K, the upper limit set to avoid softening of the quartz flow tube. We present results for two reactions over extended ranges: NF$_3$ (300–900 K) and CH$_3$Cl (600–1100 K). Electron attachment rate constants for NF$_3$ had been measured earlier using our conventional FALP apparatus. Those measurements were repeated with the FALP and then extended to 900 K with the HT-FALP. CH$_3$Cl attaches electrons too weakly to study with the low temperature FALP but reaches a value of $\sim 10^{-9}$ cm^3 s^{-1} at 1100 K. F$^-$ is produced in NF$_3$ attachment at all temperatures and Cl$^-$ in CH$_3$Cl attachment, as determined by a quadrupole mass spectrometer at the end of the flow tube. Future modifications to increase the plasma density should allow study of electron-ion recombination at high temperatures. © 2009 American Institute of Physics.
[DOI: 10.1063/1.3097185]

I. INTRODUCTION

Recent papers have highlighted the importance of electron attachment reactions in advances for such diverse applications as plasma processing, gas lasers, electrical insulation, solar energy conversion, electron-controlled chemistry, destruction of waste halocarbons, and molecular toxicity.[1–3] See also the earlier book edited by Christophorou[4] on applications of electron interactions. Most of these applications are based on the fact that electron attachment rate constants are often 100 times greater than ion-molecule ones and often many orders of magnitude greater than neutral-neutral ones. Low-energy electron attachment is also considered an initial step in radiation damage of DNA, which has led to studies of electron interactions with nucleic bases, nucleotides, and DNA itself.[5,6] Of special interest to us are electron attachment reactions in the atmosphere and in plasmas in the boundary layers of surfaces of high-speed vehicles. The latter environments are usually at high temperature. Attachment rate constants and product information are typically only available at room temperature and occasionally up to temperatures of 550 K. Extrapolation to high temperatures is uncertain. There have been a number of books and review articles on electron attachment processes.[4,7–12]

Conventional electron attachment apparatuses, such as our flowing afterglow Langmuir probe (FALP) apparatus, can be made to operate up to 550 K without a great deal of effort. Higher temperatures require greater attention to materials problems. A University of Houston group has reported electron attachment rate constants up to 600 K.[13] The Oak Ridge group has made electron attachment measurements up to 700 K in a drift tube.[14] A Boston College group extended the limit to 1022 K with a flowing-afterglow electron-cyclotron-resonance apparatus that was capable of operating as high as 1200 K.[15–17] Yale University groups have reported ion yields[18–20] from electron attachment to SF$_6$ and cross sections[21] versus electron energy for attachment to SF$_6$ and a variety of halomethanes at temperatures as high as 1200 K using electron-beam techniques.

Our laboratory relies on fast flow reactors to study plasma processes over extended temperature and pressure ranges. We have studied electron attachment reactions from 300–550 K in a FALP apparatus and ion-molecule reactions in a high temperature flowing afterglow (HTFA) from 300–1800 K, both with mass spectrometer detection of ions. Here, we describe adding a movable Langmuir probe to the HTFA so that electron attachment reactions can be studied up to 1200 K, though not many electron-attaching gases are thermally stable at such high temperatures. The first data using this modified apparatus on electron attachment to NF$_3$ (300–900 K) and CH$_3$Cl (600–1100 K) are presented. The latter reaction has not been studied at low temperatures because the rate constant is so small that any measurement would likely be dominated by impurities. An Arrhenius plot of the data yields an estimate for the room temperature rate constant of $\sim 10^{-17}$ cm^3 s^{-1}.

[a]Also at Institute for Scientific Research, Boston College, Chestnut Hill, MA.
[b]Permanent address: Department of Physics, University of Puerto Rico, Mayaguez, Puerto Rico.
[c]Author to whom correspondence should be addressed. Electronic mail: afrl.rvb.pa@hanscom.af.mil.
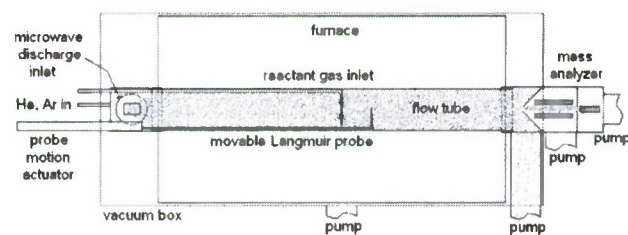
FIG. 1. (Color online) A sketch of the HT-FALP apparatus. The plasma flows from left to right in the figure.

II. EXPERIMENTAL

The new instrument, which we call the high temperature flowing afterglow Langmuir probe apparatus (HT-FALP), adds a Langmuir probe to our HTFA instrument, which has a long history in the study of ion-molecule reactions.[22–24] For more moderate temperatures, the HT-FALP overlaps with a conventional FALP in our laboratory.[11,25] Since both the HFTA and FALP have been well described individually, we will emphasize here the changes necessary to construct the combined instrument. Figure 1 shows a schematic of the HT-FALP. Ions are generated in a sidearm at right angles to the flow tube. Helium flows through a 2.5 cm OD quartz tube and is ionized by a movable microwave (Evenson-type) discharge cavity. Moving the cavity along this quartz tube allows adjustment of the plasma density in the flow tube due to the diffusion and electron-ion recombination losses that depend upon flight time. A mass-flow meter is used to measure the flow rate of helium buffer gas. Valves following the flow meter adjust buffer gas flow through the microwave discharge and downstream of it, providing additional control over the plasma density. The plasma density in the flow tube depends only weakly on microwave power (typically 15–20 W). After leaving the microwave cavity the plasma flows through a right angle bend into a vacuum box, which surrounds the HT-FALP furnace and flow tube. A stainless steel (SS) bellows then guides the plasma through a second right-angle bend into the main flow tube for reaction studies. Currently the distance from the microwave discharge to the main flow tube is 50 cm, restricting the plasma density at the beginning of the reaction zone to a few times 10^9 cm^{-3}. Initial plasma densities of $\sim 10^9$ cm^{-3} are ideal for electron attachment studies with a Langmuir probe, as reported in the present work. Initial plasma densities a decade greater are needed for studies of electron-ion and ion-ion recombination. In the future, the flight time of the plasma will be shortened, and the right angle bends eliminated, so that higher plasma densities can be achieved for measurements of recombination kinetics at high temperatures with this apparatus.

The main flow tube is a 7 cm ID quartz tube inserted into a commercial furnace separated into three zones that are heated resistively with silicon carbide rods, as described in detail in our earlier HTFA publication.[22] The reactant gas inlet is positioned in the flow tube near the middle of the furnace. For ion-molecule reactions, we have measured and calculated that by the time buffer gas approaches the reactant inlet, the centerline temperature approaches the wall temperature but is slightly lower; the centerline temperature con-

tinues to approach the wall temperature with distance/time. Since electron attachment rates often have stronger temperature coefficients than ion-molecule reactions and the kinetics is studied over shorter distances (typically <15 cm following the inlet position) than for ion molecule kinetics (the entire 50 cm from the inlet to the mass spectrometer sampling aperture), we have remeasured the temperature profile by replacing the Langmuir probe with a movable thermocouple. These tests revealed that the temperature at the inlet could be lower than the furnace temperature by as much as 5%. While the movable thermocouple was in place, we confirmed that we could obtain a uniform temperature ($\pm 1.5\%$) over the 25 cm used in attachment studies by overheating the upstream zone of the furnace, thereby transferring heat more rapidly to the buffer gas. As a result of these tests, we now have a chromel-alumel thermocouple (254 μm diameter wires) mounted at the base of the reactant inlet, 1.5 cm from the flow tube wall, and measure the gas temperature only at the entrance to the reaction zone. This measurement is needed because the amount of upstream preheating of the buffer gas depends on the gas pressure and flow rate chosen for a particular experiment.

All feedthroughs pass into the upstream end of the flow tube since it is not possible to insert tubing and wires through the furnace that surrounds the majority of the flow tube. Six 6 mm OD tubes enter a chamber at the upstream end of the main flow tube: a short SS He buffer gas tube, a short SS Ar gas tube, a quartz pressure-measurement tube that protrudes to the center of the main flow tube, a quartz reactant gas inlet tube that defines the start of the reaction zone, a quartz-insulated chromel-alumel thermocouple positioned a few millimeter upstream of the reaction zone, and the Langmuir probe tube, which moves as much as 25 cm downstream from the reactant inlet. The reactant gas tube ends in a thin quartz torus oriented perpendicular to the flow tube axis, supporting needlelike quartz injectors, which spray reactant gas radially at four points 1 cm from the axis of the flow tube. This design helps spread the attaching gas uniformly across the flow tube cross section, which reduces end corrections. Our experience is that the gas mixes quickly, i.e., within a centimeter, as determined from the shape of the electron density versus distance (flow time) plot described below. Ar gas is added in order to convert He$_2^+$ and He* (metastable-state He) to Ar$^+$,

$$\text{He}_2^+ + \text{Ar} \rightarrow \text{Ar}^+ + 2\text{He},\tag{1}$$

$$\text{He}^* + \text{Ar} \rightarrow \text{Ar}^+ + \text{e}^- + \text{He}.\tag{2}$$

The Ar addition typically increases the electron density by a factor of 2, in large part through reaction 2 and to a minor extent by reducing losses due to diffusion. Reaction 1 is important because electron-ion recombination with atomic ions (Ar$^+$) is negligible at our gas pressures, while recombination with molecular gases such as He$_2^+$ or impurity ions would result in lower plasma densities. Ar gas needs only make up 1%–2% of the buffer gas to drive reactions 1 and 2 to completion before the reaction zone, but we have used as much as 13% Ar at 1100 K because Ar reduces the ambipolar diffusion rate in the plasma. At high temperatures, larger
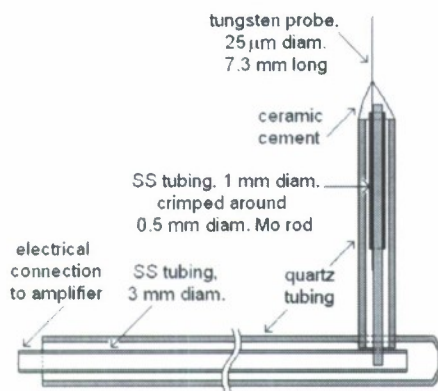
FIG. 2. (Color online) A sketch of the Langmuir probe construction (not to scale). See text for detailed description. Not shown are curved feet in and out of the plane of the drawing that keep the probe centered radially.

flows of both He and Ar are needed to keep ambipolar diffusion losses from dominating over electron attachment decay of the electron density. Increased He flow results in greater velocities in the flow tube and therefore less time for diffusion. (We aim for conditions in which diffusion accounts for no more than one-third of the decay in the electron density, and electron attachment the rest.) He flows increase from 18 000 to 30 000 std. cm³ per min (SCCM) and Ar from 400 (~2%) to 4600 (~13%) SCCM as one goes from 500 to 1100 K. The experiment is gas intensive, with a size 1A cylinder of He (6.9 atm m³) only lasting 4–7 h. This unfortunate feature of the apparatus is largely historical; in the early 1990s the HTFA flow tube size was modeled on that used by Ferguson et al.,[26] chosen so that diffusion losses were tolerable. Because the HTFA was to operate at even higher temperatures, where diffusive losses are greater, the historical size was kept. For the present HT-FALP, the flow tube size was not decreased because the Langmuir probe and toroidal inlet modifications meant inserting additional parts through the open end of the HTFA flow tube. Recent experiments with smaller diameter and shorter flow tubes have shown that accurate kinetics measurements are possible with much less gas flow, at least near room temperature.[27,28] Those experiments, combined with lessons from the present work, may make it possible to construct a HT-FALP with more conservative gas flow.

The Langmuir probe construction is shown schematically in Fig. 2. The probe itself is a 25 μm diameter tungsten wire, which is crimped to the side of a 500 μm diameter molybdenum wire using a 1 mm ID SS tube, 2 cm in length. The tungsten wire protrudes some desired length to act as a cylindrical Langmuir probe. The probe and connector are inserted into a 4 mm OD quartz tube to insulate the connector assembly from the plasma. A small portion of the connector extends beyond the quartz tube and is coated with Al₂O₃ paste to provide more compact insulation at the probe base. This assembly is mounted radially so that the Langmuir probe (presently 7.3 mm in length) is centered on the flow tube axis. The probe connector assembly fits at right angle into one end of a 3 mm diameter SS tube, which runs a 76 cm distance upstream in the flow tube for electrical connection to the outside world. This SS tubing is insulated with

6 mm OD quartz tubing, which has curved feet (not shown in Fig. 1) to keep the probe pointing radially at all times. At the cool end of the apparatus this entire assembly is coupled to a linear manipulator, providing electrical connection using a spring-loaded spool to prevent wire coiling as the probe is moved along the flow tube. The manipulator allows the probe to be moved 25 cm along the flow tube using a stepping motor.

In order to measure electron densities, the voltage on the Langmuir probe is swept and the electron density is derived from the cylindrical probe equation developed by Langmuir and Mott-Smith[29]

$$I = Ae[e^-]\pi^{-1}\{2m_e^{-1}[kT_e + e(V - V_p)]\}^{1/2}, \qquad (3)$$

where I is the current collected from the plasma, A is the area of the probe exposed to the plasma, $[e^-]$ is the electron number density, m_e is the electron mass, k is Boltzmann's constant, T_e is the electron temperature in the plasma (equal to the gas temperature in the present work), V is the positive potential applied to the probe, and V_p is the plasma potential. V_p is nominally ground potential, but contact potentials between metals and sheath potentials yield a V_p that can be 0–2 V off of ground potential. It is conventional to plot the square of the current because of the linear dependence of I^2 upon V for values of $V \gg kT_e$, which is easily fit to determine $[e^-]$ without needing to specify T_e and V_p. Note that Eq. (3) assumes that charged particles suffer no collisions in traversing the plasma sheath around the probe, which limits gas pressures to a few Torr for electrons and much less than a Torr for ions. Our attachment data are collected and analyzed using methods and software developed by Španěl.[30]

Figures 3(a) and 3(b) show I^2 versus V plots at 500 and 1000 K, respectively. The 500 K Langmuir probe characteristics are typical of what are observed in our low temperature FALP apparatus. At negative probe potentials, positive ions are collected, and the probe current is in the nanoampere range. When the more mobile electrons are collected with positive probe potentials, typically several microampere of current are collected from the plasma. The result is the plot shown in Fig. 3(a) with an essentially flat portion (positive ions) on the left-hand side, and a steeply rising portion on the right due to electron collection. Note that the crossover point between positive ion collection and electron collection is not at zero applied potential because of contact potentials. The slope of the linear part of these plots yields the absolute electron density $[e^-]$ through Eq. (3), although only relative densities are needed to derive attachment rate constants (if recombination can be neglected). At high temperatures (≥ 900 K), the profile changed as shown in Fig. 3(b) for 1000 K. In this profile, the expected flat portion is slightly elevated from zero current, and there is distortion on the positive-ion (left side) of the characteristic. Perhaps this indicates a problem due to thermionic emission or a small leakage current as insulators become somewhat conducting at high temperatures. Modeling thermionic emission of alkali ions from the probe is nontrivial because ions can be removed both by gas flow and by the probe bias relative to ground potential. Still, the right-hand side of the curve is what is typical for electron collection, and the resulting $[e^-]$
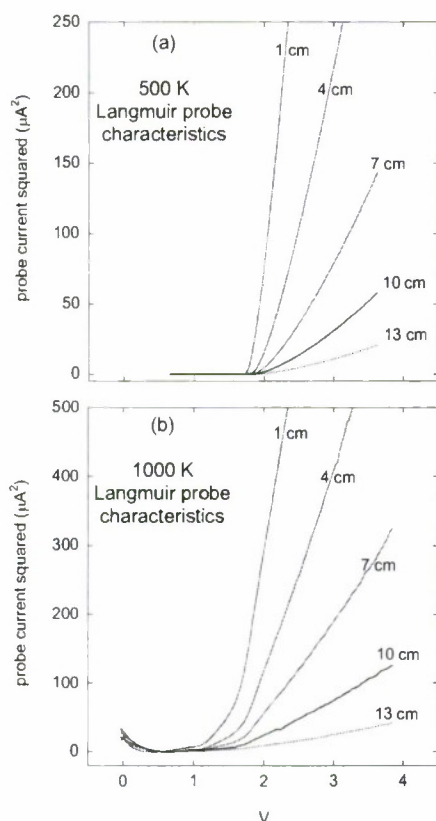
FIG. 3. (Color online) (a) Langmuir probe I^2 vs V characteristics obtained at 500 K with attaching gas present. Fits to the linear portion on the right side yield electron densities (in 10^8 cm^{-3} units): 24.2 (1 cm), 15.3 (4 cm), 9.46 (7 cm), 6.04 (10 cm), and 3.60 (13 cm). (b) Similar for 1000 K: 15.3 (1 cm), 10.5 (4 cm), 6.89 (7 cm), 4.21 (10 cm), and 2.52 (13 cm).

are adequate for attachment kinetics to be derived. One reason we are comfortable with the measurements of $[e^-]$ despite the distortions at low potentials is that measurement of the ambipolar diffusion rate seems unexceptional at high temperatures. With no reactant gas present, we measure $[e^-]$ as a function of distance (time) along the flow tube, and find the expected exponential dependence, described by a rate consistent with those extrapolated from lower temperatures. The precise values of these diffusion coefficients are not presented because the flows and pressures of He and Ar were not fixed in any consistent manner. A separate study of the diffusion coefficients with systematically varied conditions would be useful.

An additional problem occurring at temperatures ≥ 900 K is increased noise in the I^2 versus V profiles, which makes it more difficult to measure low electron concentrations ($\lesssim 2 \times 10^8$ cm^{-3}). If in the future, we reach the point of measuring electron-ion recombination rate constants at high temperatures, further work will be required to ensure the correctness of absolute values of $[e^-]$. However, it is possible that the higher $[e^-]$ needed for recombination studies will cause these issues to be less important, as I^2 will be substantially larger.

The plasma flows into a mass spectrometer sampling orifice at the end of the flow tube. Most of the gas is pumped away by a Roots blower, but a small fraction is sampled through a 0.3 mm pinhole into an Einzel lens, followed by a

rf-electric quadrupole mass spectrometer and a discrete-dynode electron multiplier. The attachment reactions presented here have produced only one product ion, confirmed by the mass spectra. Small impurities levels of CN$^-$, Cl$^-$, and a few other species are also present, especially at our highest temperatures. However, those ions contribute only a few percent of the negative ion signal at most. The positive ion spectra in the absence of attaching gas are dominated by Ar$^+$. Under some conditions, He$^+$ is present at the 10%–30% level. A consistent H$_2$O$^+$ impurity at about 10% of the Ar$^+$ signal is observed. Other minor mass peaks formed from air are also present. Some of the impurities come from leaks since the flow tube seals at high temperature are not perfect. The entire flow tube and furnace sit inside of a vacuum box pumped by a second Roots pump. The pressure in the vacuum box, which contains fire bricks, is typically $<5\%$ of the flow tube pressure. Without this outer chamber, leaks would be large enough to prevent operation of the HT-FALP.

Velocity measurements are made by pulsing the discharge and measuring the time for the disturbance to reach the Langmuir probe at different distances. The plasma velocity exceeds the bulk gas velocity because the plasma density profile across a flow tube diameter overlaps more of the peak in the buffer gas parabolic (laminar flow) profile. The velocity measurements were carried out for a variety of flow rates at different temperature and pressures, giving a ratio of plasma velocity to bulk gas velocity of 1.7. This factor was then used routinely.

NF$_3$ gas (99.8% purity) was obtained from Ozark-Mahoning of Tulsa, Oklahoma. The major impurities are said to be nonattaching gases in our energy range, e.g., CF$_4$, O$_2$, and Ar, but there may be a few parts per million by volume of SF$_6$. Our CH$_3$Cl gas (99.9% purity) was obtained from Matheson Tri-Gas of Basking Ridge, New Jersey. NF$_3$ is commonly used as a fluorine source for silicon etching. Largely because of the rising demand for flat panel displays, production of NF$_3$ is expected to reach 4000 tons in 2008. It is estimated that 2%–3% escapes into the atmosphere, which is a problem because NF$_3$ has an atmospheric lifetime of 550 yr with a 20 yr global warming potential of 12 200 times that of CO$_2$.[31]

III. KINETICS DATA

In order to derive rate constants for electron attachment, electron concentrations are measured along the axis of the flow tube with and without the attaching gas present. The measurements start about 1 cm downstream of the attaching-gas inlet since it is not physically possible in the present arrangement to have the Langmuir probe pass under the inlet, as it does in the low-temperature FALP.

Figure 4 shows axial electron concentrations as a function of reaction time for a typical data run at 1000 K with CH$_3$Cl. Because some of the rate constants measured in this work are small enough that a correction is required for electron-ion recombination, the rate equations below will include the ion-molecule reaction between Ar$^+$ and the reactant

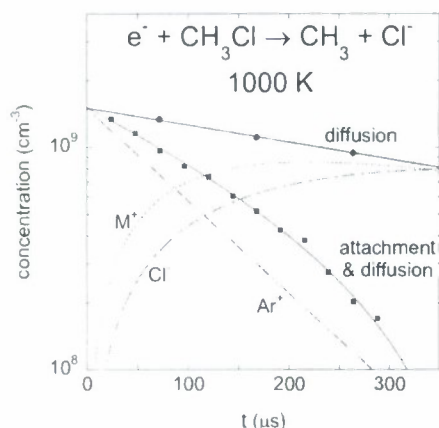FIG. 4. (Color online) Data obtained with the HT-FALP at 1000 K for electron attachment to CH_3Cl. The diffusion data were obtained in absence of CH_3Cl. The smooth lines for diffusion, attachment and diffusion, and Ar^+, Cl^-, and M^+ concentrations are solutions to the rate equations given in Eqs. (4)–(7). M^+ represents products of the $Ar^+ + CH_3Cl$ reaction, with loss due to diffusion and slightly to electron-ion recombination.

FIG. 5. (Color online) Data for $[e^-]$ vs reaction time at 1000 K in 1.45 $\times 10^{16}$ cm^{-3} of He and Ar buffer gas. The upper line shows ambipolar diffusion loss (1634 s^{-1}) obtained without CH_3Cl present. The lower curves show the coupled effect of diffusion and electron attachment for two concentrations of CH_3Cl gas, (a) 4.95×10^{12} cm^{-3} and (b) 3.60×10^{12} cm^{-3}. Curve (a) was calculated with $k_a = 7.8 \times 10^{-10}$ cm^3 s^{-1} and curve (b) with 8.2×10^{-10} cm^3 s^{-1}.

molecule M (NF_3 or CH_3Cl here), which yields a molecular ion (NF_2^+ or CH_3^+ and CH_2Cl^+ along with secondary ions) denoted by M^+.

$$d[Ar^+]/dt = -k_{im}[Ar^+][M] - v_D[Ar^+] \tag{4}$$

$$d[M^+]/dt = +k_{im}[Ar^+][M] - k_r[e^-][M^+] - v_D[M^+] \tag{5}$$

$$d[Cl^-]/dt = -k_a[e^-][M] \tag{6}$$

$$d[e^-]/dt = d[Ar^+]/dt + d[M^+]/dt - d[Cl^-]/dt. \tag{7}$$

Here, square brackets indicate concentrations of neutrals, ions, and electrons, and k_{im} is the ion-molecule reaction rate constant, k_a is the electron attachment rate constant, k_r is the electron-ion recombination rate constant, and v_D is the measured ambipolar diffusion frequency, measured in absence of attaching gas. First-order kinetics is assumed, i.e., $[M] \gg [e^-]$, so any change in $[M]$ is negligible. Because the recombination correction is mostly an issue at low temperatures due to the steep temperature dependences of the attachment reactions, it is sufficient to take k_{im} as the collisional rate constant as calculated using the model of Su and Chesnavich,[32] and to estimate the recombination rate constant as $3 \times 10^{-7}(300/T)^{1/2}$ cm^3 s^{-1}. Rate constants for the reaction $Ar^+ + NF_3 \rightarrow F + NF_2^+$ have been measured over the range 300–550 K and found to be collisional.[33] Smith et al.[34] measured essentially collisional rate constants for reaction of Ar^+ with both NF_3 and CH_3Cl at 297 K.

The rate Eqs. (4)–(7) have a simple solution if electron-ion recombination can be ignored,[11,12]

$$[e^-] = [e^-]_0 \{v_a \exp(-v_a t) - v_D \exp(-v_D t)\}/(v_a - v_D), \tag{8}$$

where $[e^-]_0$ is the initial electron density at $t=0$, and v_a is the attachment frequency, related to the attachment rate constant by $k_a = v_a[M]$.

Note that Eq. (6) does not include a diffusion term, since negative ions cannot compete with the much more mobile electrons in ambipolar-diffusion-controlled plasmas. As the negative ion concentration builds up in time, the electrons
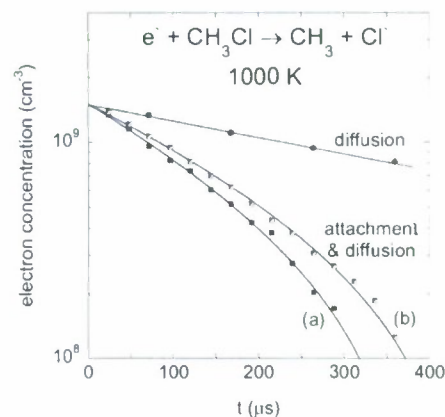
take on a greater burden matching the diffusive loss of Ar^+, which eventually leads to sudden loss of remaining electrons. Equation (7) simply expresses charge neutrality in the plasma. For slow electron attachment rates, when large quantities of neutral reactant are added (still, $\approx 0.1\%$ of the buffer gas concentration), Ar^+ may be converted into molecular ions, which can recombine with electrons to a significant degree even for $[e^-]_0$ near 10^9 cm^{-3}. For this reason, the plasma densities are kept low ($\sim 10^9$ cm^{-3}), and modeling using Eqs. (4)–(7) is used to correct for recombination events for electron attachment rate constants below about 10^{-10} cm^3 s^{-1}. The importance of recombination decreases with increasing temperature since recombination rates decrease approximately as $T^{-1/2}$. The smooth curves shown in Fig. 4 are the model fits using Eqs. (4)–(7). Data were obtained with at least two concentrations of reactant gas at each temperature. The rate constants obtained from the two measurements agree within 10%. Figure 5 shows the data of Fig. 4 together with those for a second concentration of CH_3Cl gas. As a test of the kinetics modeling, some data were also obtained by fixing the Langmuir probe at a certain distance from the reactant gas inlet, e.g., 6 cm downstream, and varying the concentration of reactant. Such data were found to yield the same result as with the variable-distance, fixed $[M]$, method. (The analysis is slightly more involved as the rate equations must be solved for each $[M]$ instead of once for a single $[M]$.)

Uncertainties in rate constants obtained with the current instrument are similar to those with the FALP. We estimate that an additional 5% uncertainty is needed for the data at 1000 K and above where the Langmuir probe plots have higher scatter. Typical uncertainties are $\pm 25\%$ for absolute error and $\pm 15\%$ for the relative error between temperatures. As noted below, a still larger uncertainty may be assigned for data requiring a large electron-ion recombination correction.

IV. RESULTS AND DISCUSSION

Electron attachment rate constants for NF_3 were measured 13 yrs ago in our FALP apparatus.[35] The FALP experi-

TABLE I. Electron attachment rate constants k_a for NF_3 obtained with the FALP apparatus and the new HT-FALP apparatus in the present work. The experimental uncertainty is $\pm 25\%$ except for the 300 K datum ($\pm 50\%$).

T (K)	FALP k_a (cm^3 s^{-1})	HT-FALP k_a (cm^3 s^{-1})
300	5.0×10^{-12}	$\cdots$
363	1.7×10^{-11}	$\cdots$
425	5.2×10^{-11}	$\cdots$
500	1.2×10^{-10}	1.4×10^{-10}
550	2.8×10^{-10}	$\cdots$
600	$\cdots$	4.1×10^{-10}
700	$\cdots$	9.2×10^{-10}
808	$\cdots$	1.9×10^{-9}
851	$\cdots$	1.5×10^{-9}
900	$\cdots$	1.6×10^{-9}

TABLE II. G3 results for the NF_3 and CH_3Cl systems.

Molecule	Total energy, Neutral (0 K, hartree)	Total energy, negative ion (0 K, hartree)	Electron affinity, from G3 (0 K, eV)
F	$-99.684\ 21$[a]	$-99.809\ 19$[a]	3.401[b]
NF	$-154.371\ 15$	$-154.377\ 49$	0.172
NF_2	$-254.158\ 22$	$-254.199\ 50$	1.123[c]
NF_3	$-353.932\ 73$[a]	$-353.977\ 19$	1.210
Cl	$-459.990\ 96$[a]	$-460.123\ 60$[a]	3.609[d]
CH_3	$-39.793\ 30$[a]	$-39.791\ 85$[a]	0.039[e]
CH_3Cl	$-499.913\ 02$	None	$\cdots$

[a]Ref. 37.
[b]Experiment: $3.401\ 189\ 5 \pm 0.000\ 002\ 5$ eV, Ref. 40.
[c]Experiment: 1.1 ± 0.1 eV from electron attachment threshold in Ref. 39.
[d]Experiment: $3.612\ 724 \pm 0.000\ 027$ eV, Ref. 41.
[e]Experiment: 0.08 ± 0.03 eV, Ref. 42.

ment was repeated for the present work since a number of improvements have been made in the apparatus, notably in the temperature uniformity in the reaction zone.[36] Table I lists results obtained for NF_3 using the new HT-FALP (500–900 K) apparatus along with the new FALP data (300–550 K). The agreement between the two sets of data is quite good. Agreement with the 1995 results is good except values at 462–551 K, which are as much as a factor of 2 higher than the new data and do not quite follow the same trend, as shown in Fig. 6. We cannot explain the discrepancy for those data points. At temperatures below 500 K, appreciable corrections for electron-ion recombination have been made. At 300 K, the correction is particularly large with the apparent rate constant changing from 1.3×10^{-11} cm^3 s^{-1}, if recombination is not recognized, to a correct value of 5×10^{-12} cm^3 s^{-1}. Here is a case where the measurement uncertainty increases substantially, perhaps to $\pm 50\%$. By 500 K, the electron-ion correction is only $\sim 10\%$. The corrections continue to be smaller with increasing temperature because the attachment rate constant increases substantially with temperature (meaning that a smaller NF_3 concentration is needed, and hence fewer molecular positive ions are formed) and because recombination has a negative temperature dependence.
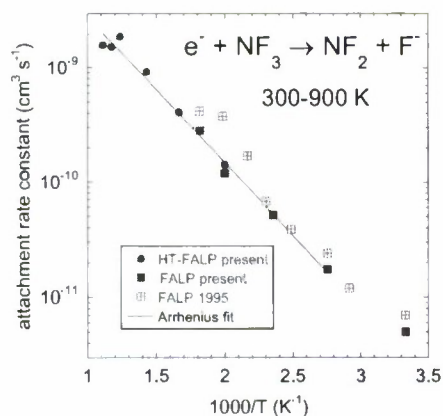

FIG. 6. (Color online) Arrhenius plot of NF_3 attachment data obtained with the FALP and new HT-FALP apparatus, compared to data obtained with the FALP apparatus in 1995 (Ref. 32). The Arrhenius fit does not include earlier data and omits the room temperature datum.

The only exothermic channels possible for NF_3 are dissociative attachment yielding F^-, Eq. (9), and nondissociative attachment, yielding the NF_3^- parent ion. F^- is the sole product ion observed within our 1% detection limit.

$$e^- + NF_3 \rightarrow F^- + NF_2 + 0.94 \ \text{eV}. \tag{9}$$

The exothermicity given above at 0 K is from calculations carried out using the G3 compound method of Curtiss *et al.*,[37] using the Gaussian–03W computer program.[38] The G3 method has an average accuracy of ± 0.091 eV for ionization energies, electron affinities, and heats of formation for nonhydrogen molecules (and half that for hydrogen-containing molecules).[37] The G3 electron affinity of NF_3 is 1.21 eV, but it is apparent that the nascent NF_3^- cannot be stabilized before autodetaching or dissociating, under the conditions of the FALP and HT-FALP experiments. The NF_3^- parent ion was observed for the first time by Ruckhaberle *et al.*[39] in evaporative electron attachment to NF_3 clusters. G3 energies for molecules needed in the calculation of reaction energetics are tabulated in Table II. G3 and experimental[39–42] electron affinities are also listed in Table II.

With all data included, the activation energies determined with the FALP and HT-FALP from Arrhenius fits (Fig. 6) are 0.22 and 0.25 eV, respectively. Omitting the FALP room temperature datum (which includes a large electron-ion recombination correction), both sets of data give the same activation energy, 0.25 ± 0.05 eV. The 1995 FALP data show a somewhat larger activation energy, 0.29 eV (which was rounded to 0.30 ± 0.06 eV for publication[35]), because of the data at 462–551 K, which appear now to be erroneously high. The Arrhenius pre-exponential factor for the combined FALP and HT-FALP data is 5.3×10^{-8} cm^3 s^{-1}. The pre-exponential factor (which is very sensitive to the Arrhenius slope) is smaller than the collisional rate constant, which varies from 2.39×10^{-7} cm^3 s^{-1} at 300 K to 1.83×10^{-7} cm^3 s^{-1} at 900 K, including the small contribution of the dipole moment (a fraction of a percent).[43] The good agreement between the present FALP and HT-FALP data implies that the new instrument works well at high temperature.

The electron-beam experiment of Ruckhaberle *et al.*[39] with NF_3 clearly showed a zero-energy resonance for the production of F^-, which grew as the NF_3 temperature was

TABLE III. Electron attachment rate constants k_a for CH_3Cl obtained with the new HT-FALP apparatus in the present work. The experimental uncertainty is $\pm 25\%$ for 700–900 K and $\pm 30\%$ for the 600, 1000, and 1100 K data.

T (K)	k_a ($cm^3 \ s^{-1}$)
700	2.3×10^{-11}
800	9.3×10^{-11}
900	3.6×10^{-10}
1000	7.9×10^{-10}
1100	9.8×10^{-10}

increased from 296 to 552 K. The growth of the F^- was said to show an activation energy of 0.10 ± 0.05 eV. Ruckhaberle et al.[39] described this result as incompatible with the larger activation energy of the 1995 FALP experiment, and consequently with the present 0.25 ± 0.05 eV. Ruckhaberle et al.[39] acknowledged that there is a difference between the two experiments in that their activation energy corresponded to a nominal electron energy of 0 eV, while the FALP experiment is truly thermalized, i.e., the average electron energy follows $3kT/2$, and hence increases from 0.039 to 0.12 eV in the present work with NF_3. Ruckhaberle et al.[39] supported their low activation energy with density functional calculations on the change in NF_3 potential energy for N–F stretching motion, which yielded an activation energy of 0.2 eV, believed an overestimate. Aside from a question of whether such a calculation is accurate enough to choose between the rival experimental activation energies, there are more important issues noted by Fabrikant and Hotop[44] in a recent study of Arrhenius-like behavior in electron attachment. Fabrikant and Hotop[44] found that the activation energy determined from thermal attachment depended on whether the reaction was endothermic or exothermic. If exothermic, as in the NF_3 case, the activation energy determined from an Arrhenius plot underestimated the barrier energy by a degree that depended upon the active vibrational energy. Even then, the actual barrier height was uncertain because the theoretical barrier energy requires knowledge of the diabatic anion potential energy surface.[44] For NF_3, a symmetric deformation vibration[45] at 647 $cm^{-1} = 40$ meV seems most likely to promote dissociative attachment. Table III of Fabrikant and Hotop[44] and Fig. 6 give model data for a hypothetical molecule with a vibrational energy of 43 meV, and those data indicate that the activation energy of 0.25 eV measured in the present work results from a barrier of 0.35 eV.

Ruckhaberle et al.[39] also reported weak signals of F_2^- and NF_2^- produced in less than 0.1% of NF_3 attachment reactions, values too small for us to confirm with the HT-FALP. However, our G3 calculations show these attachment channels to be 0.69 and 1.33 eV endothermic at 0 K, respectively. Aside from F^- production from a zero-energy resonance, F^-, F_2^-, and NF_2^- are also observed in the beam experiment seem to arise from a resonance around 2 eV. The increases in F^- ion signal observed by Ruckhaberle et al.[39] with electron energy are considerably smaller than the temperature dependence observed in the present work, indicating that vibrational energy is the dominant factor behind the activation energy.
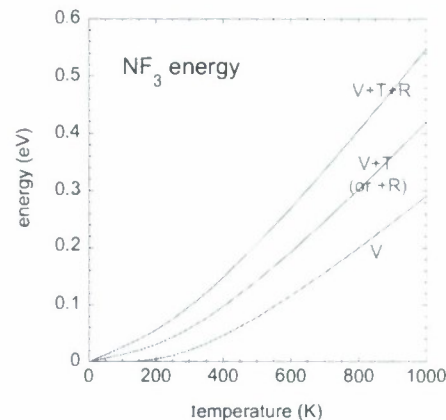

FIG. 7. (Color online) Energy in the NF_3 molecule vs temperature. The label V is for vibrational energy; $V+T$ (or $+R$) represents vibrational plus translational energy (equivalently, vibrational plus rotational); and $V+T+R$ represents all three forms of energy.

Figure 7 shows the energy in the system as a function of temperature. Included are curves for vibrational energy only, vibrational energy plus either translational or rotational energy, and all three forms. However, rotational energy probably plays little role since the attachment process is likely s-wave dominated. If vibrations are thought to be the cause of the steep temperature dependence, it is useful to compare with NF_3 frequencies. All NF_3 frequencies[45] are too small to explain the activation energy, but two quanta of stretches match quite well, implying that the curves cross near $v = 2$. A detailed analysis is beyond the scope of this instrumental paper.

Electron attachment to CH_3Cl has one exothermic channel,

$$e + CH_3Cl \rightarrow Cl^- + CH_3 + 0.11 \ eV, \tag{10}$$

where the exothermicity (0 K) is from a G3 calculation. We prefer quoting the G3 result instead of using NIST data[45] because the latter requires mixing of 298 K heats of formation with 0 K electron affinities to evaluate the low exothermicity of reaction (10). Use of NIST data for reaction (10) yields an exothermicity of 0.02 eV, e.g., nearly thermoneutral. Furthermore, we wished to evaluate the exothermicity of reaction (10) as a function of temperature, which the G3 method readily permits. The resulting reaction enthalpies are 0.105 eV (0 K), 0.098 eV (298 K), and 0.034 eV (1000 K), including the enthalpy of the electron.

Electron attachment data for CH_3Cl (600–1100 K) are given in Table III, and the results are shown in Arrhenius form in Fig. 8. It was impractical to obtain data below 600 K due to the large temperature dependence of the rate constant. For example, at 500 K the rate constant would be only 3.3 $\times 10^{-13}$ $cm^3 \ s^{-1}$ if the Arrhenius behavior is followed. The fit to the data shown in Fig. 8 omits the 1100 K datum and yields an activation energy of 0.67 ± 0.07 eV, where the uncertainty reflects fits within the 15% relative error bars shown in the figure. (Including the 1100 K datum gives an activation energy of 0.64 eV.) The pre-exponential factor is 1.7×10^{-7} $cm^3 \ s^{-1}$ for the fit shown, a value that is lower than the collisional rate constants calculated for CH_3Cl in
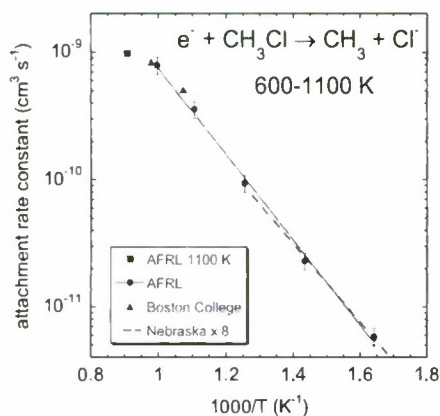
FIG. 8. (Color online) Arrhenius plot of CH_3Cl attachment data obtained with the HT-FALP apparatus. The error bars indicate ±15% relative uncertainty. Also shown are two unpublished data (triangular points) from Ref. 17 and the theoretical results of Wilde *et al.* (Ref. 46) multiplied by a factor of 8 (dashed line, Ref. 47).

this temperature range, which are 3.04×10^{-7} to 2.34×10^{-7} cm^3 s^{-1} (600 and 1100 K, respectively).[43] Note that the collisional rate constants given here are ~30% larger than what one would obtain if the dipole moment (1.8963 D) of CH_3Cl were to be ignored.[43]

The fact that the 1100 K point is slightly below the trend from the lower temperature data may indicate that ~10%–20% of the CH_3Cl is decomposing at high temperature. While Ko *et al.*[48] indicated that temperatures under 1200 K are acceptable with CH_3Cl, we note that the preheating zone of the HT-FALP exceeds that temperature in order to achieve 1100 K in the reaction zone and the CH_3Cl passes through an inlet tube in contact with the flow tube walls, which are at the higher temperature. We have no independent way of determining whether that decomposition is occurring. Thus, at this juncture we cannot rule out the possibility that the 1100 K measurement may represent an unknown problem in the experiment at 1100 K rather than non-Arrhenius behavior for CH_3Cl attachment.

Total electron scattering cross sections have been measured by Jones *et al.*[49] with CH_3Cl at 300 K temperature. Those measurements gave a cross section of 1.54×10^{-17} m^2 at an electron energy corresponding to 300 K. Electron attachment is an infinitesimal contribution to this large cross section. There have been electron beam and drift tube studies of electron attachment to CH_3Cl; see Pearl *et al.*[50] (500–750 K), Datskos *et al.*[51] (400–750 K), and Petrovic *et al.*[47] (295 K). Pearl *et al.*[50] note that CH_3Cl can decompose to HCl on a heated SS surface. They pointed out that because of the small attachment rate constant for CH_3Cl, only a small fraction need decompose to cause experimenters to mistakenly attribute a peak in the HCl cross section at 0.8 eV to CH_3Cl. The zero-energy resonance is unaffected, since attachment to HCl is endothermic, meaning that decomposition of CH_3Cl will lead to lower thermal rate constants by an amount commensurate with the lost CH_3Cl. Drift tube data of Datskos *et al.*[51] do not extend to thermal electron energies and must be extrapolated to obtain rate constants for comparison with the present results. The extrapolation is not unique because some of the data show a

peak in the rate constant at very low energies. Our extrapolations, smoothing those peaks, give thermal rate constants that are higher than the present ones by factors of 2.3 (600 K) to 1.4 (750 K).

Fabrikant[52] carried out R-matrix calculations of the attachment cross section for CH_3Cl. The calculation accounted explicitly only for the C–Cl stretch vibration, and was put on an absolute scale by matching the shape and peak vibrational excitation cross section measured by Shi *et al.*[53] The calculated attachment cross sections plotted versus electron energy displayed prominent vibrational features (20–60 meV in width) associated with vibrational Feshbach resonances. The cross sections increased dramatically with CH_3Cl temperature, most significantly for the lowest vibrational levels. Pearl *et al.*[50] compared these cross sections with their electron-beam data by folding the calculated cross sections with a 67 meV Gaussian electron energy distribution. While this process washed out the vibrational structure, the calculated cross sections matched the shape of the cross sections measured versus electron energy by Pearl *et al.*[50] with reasonable agreement on absolute magnitude. Wilde *et al.*[46] have extended the R-matrix work to CH_3Br and CH_3I and calculated attachment rate constants versus temperature, including those for CH_3Cl recalculated over a finer energy grid. The comparisons are interesting. Attachment rate constants for CH_3I barely change with temperature, as previously observed experimentally, with a small activation energy (~25 meV).[50] Those for CH_3Br show a much greater change with temperature, in a way that may be described by an activation energy of 250 meV, again in agreement with experiment.[46] Those for CH_3Cl show a still greater change with temperature, giving an activation energy of 611 meV, which compares reasonably well with the present experiment (666 meV with the 1100 K point omitted, or 635 meV if included). However, we had to multiply the theoretical rate constants by a factor of 8 to get them on the plot of our experimental results in Fig. 8. A factor of 8 is not as surprising as it might normally be, given the eleven order-of-magnitude change in the attachment rate constant calculated for CH_3Cl in the 200–800 K range.[46] Gallup and Fabrikant[54] recently revisited the methyl halide problem, treating more accurately the dipole moment change with C–Cl distance and including the influence of the molecular polarizability, focusing on the vibrational Feshbach resonances in relation to elastic and inelastic scattering of electrons. These features have been observed in high resolution experiments with CH_3Br and CH_3I.[55,56] Electron attachment to CH_3Cl has also been studied in a cryogenic Kr matrix by Nagesha *et al.*,[57] and that problem has been addressed theoretically by Fabrikant.[58]

The CH_3Cl data set shows a second utility of the HT-FALP, namely, enabling studies of molecules whose attachment rate constants are too slow to measure at lower temperatures. Extrapolation to 300 K yields an expected rate constant of ~10^{-17} cm^3 s^{-1}. No current apparatus is capable of making a measurement of such a slow reaction. Even if technically possible, interferences from impurities as low as a part in 10^{10} could prevent a reliable measurement.

V. CONCLUSIONS

A new instrument for measuring thermal electron attachment rate constants at temperatures up to 1200 K is described in detail. The first measurements on NF_3 and CH_3Cl are presented. Good agreement for the NF_3 data with measurements from our well established lower temperature instrument shows the accuracy of the technique. The CH_3Cl attachment kinetics cannot be measured at low temperatures since the rate constant is so small. In any case, we have shown that measurements of electron attachment rate constants up to 1100 K are possible. For highly stable molecules, such as HCl or HBr, 1200 K may be possible, but we expect that 1200 K is about the practical limit with a flow tube reactor. Future improvements are planned to increase the plasma densities so that electron-ion recombination experiments at high temperature will also be possible.

ACKNOWLEDGMENTS

[1] L. G. Christophorou, A. Zaras, and P. Papagiannakopoulos, Int. J. Mass Spectrom. **277**, 26 (2008).

[2] N. J. Mason, Int. J. Mass Spectrom. **277**, 31 (2008).

[3] L. G. Christophorou and D. Hadjiantoniou, Chem. Phys. Lett. **419**, 405 (2006).

[4] *Electron-molecule Interactions and Their Applications*, edited by L. G. Christophorou (Academic Press, New York, 1984), Vols. 1–2.

[5] Y. Zheng, J. R. Wagner, and L. Sanche, Phys. Rev. Lett. **96**, 208101 (2006); B. Boudaïffa, P. Cloutier, D. Hunting, M. A. Huels, and L. Sanche, Science **287**, 1658 (2000).

[6] P. Schyman and A. Laaksonen, J. Am. Chem. Soc. **130**, 12254 (2008).

[7] L. G. Christophorou and J. K. Olthoff, *Fundamental Electron Interactions with Plasma Processing Gases* (Kluwer Academic/Plenum Publishers, New York, 2004).

[8] H. Hotop, M.-W. Ruf, M. Allan, and I. I. Fabrikant, Adv. At., Mol., Opt. Phys. **49**, 85 (2003).

[9] A. Chutjian, A. Garscadden, and J. M. Wadehra, Phys. Rep. **264**, 393 (1996).

[10] L. G. Christophorou and J. K. Olthoff, J. Phys. Chem. Ref. Data **29**, 267 (2000).

[11] T. M. Miller, Adv. At., Mol., Opt. Phys. **51**, 299 (2005).

[12] D. Smith and P. Španěl, Adv. At., Mol., Opt. Phys. **32**, 307 (1994).

[13] L. A. Ayala, W. E. Wentworth, and E. C. M. Chen, J. Phys. Chem. **85**, 768 (1981).

[14] P. G. Datskos, L. G. Christophorou, and J. G. Carter, J. Chem. Phys. **97**, 9031 (1992).

[15] S. J. Burns, J. M. Matthews, and D. L. McFadden, J. Phys. Chem. **100**, 19436 (1996).

[16] R. G. Levy, S. J. Burns, and D. L. McFadden, Chem. Phys. Lett. **231**, 132 (1994).

[17] A preliminary description of the Boston College experiments, in an apparatus capable of reaching 1200 K, was given by D. L. McFadden, "Chemical Kinetics and Atmospheric Modification," Final Report No. PL-TR-94–2164, 1 May 1994, available online from the Defense Technical Information Center at http://handle.dtic.mil/100.2/ADA283304.

[18] C. L. Chen and P. J. Chantry, Bull. Am. Phys. Soc. **15** (3), 418 (1970).

[19] C. L. Chen and P. J. Chantry, Bull. Am. Phys. Soc. **17** (3), 406 (1972).

[20] C. L. Chen and P. J. Chantry, J. Chem. Phys. **71**, 3897 (1979).

[21] D. Spence and G. J. Schulz, J. Chem. Phys. **58**, 1800 (1973).

[22] P. M. Hierl, J. F. Friedman, T. M. Miller, I. Dotan, M. Menendez-Barreto, J. V. Seeley, J. S. Williamson, F. Dale, P. L. Mundis, R. A. Morris, J. F. Paulson, and A. A. Viggiano, Rev. Sci. Instrum. **67**, 2142 (1996).

[23] T. M. Miller, J. F. Friedman, M. Menendez-Barreto, A. A. Viggiano, R. A. Morris, A. E. S. Miller, and J. F. Paulson, Phys. Scr., T **T53**, 84 (1994).

[24] A. A. Viggiano and S. Williams, in *Advances in Gas Phase Ion Chemistry*, edited by N. G. Adams and L. M. Babcock (Academic, New York, 2001), Vol. 4, p. 85.

[25] J. F. Friedman, T. M. Miller, J. K. Friedman-Schaffer, A. A. Viggiano, G. K. Rekha, and A. E. Stevens, J. Chem. Phys. **128**, 104303 (2008).

[26] E. E. Ferguson, F. C. Fehsenfeld, and A. L. Schmeltekopf, Adv. At. Mol. Phys. **5**, 1 (1969).

[27] T. Wang, D. Smith, and P. Španěl, Int. J. Mass Spectrom. **272**, 78 (2008).

[28] D. Smith, A. Pysanenko, and P. Španěl, Int. J. Mass Spectrom. **281**, 15 (2009).

[29] I. Langmuir and H. M. Mott-Smith, Gen. Electr. Rev. **27**, 449 (1924); H. M. Mott-Smith and I. Langmuir, Phys. Rev. **28**, 727 (1926).

[30] P. Španěl, Int. J. Mass Spectrom. Ion Process. **149–150**, 299 (1995).

[31] M. J. Prather and J. Hsu, Geophys. Res. Lett. **35**, L12810 (2008).

[32] T. Su and W. J. Chesnavich, J. Chem. Phys. **76**, 5183 (1982); T. Su, *ibid.* **89**, 5355 (1988); **88**, 4102 (1988); We used the parameterized formula given in the final citation, except that the dimensionless temperature T_R is misprinted; $T_R = 2ak_B T / \mu_D^2$. In this calculation for CH_3Cl we used a polarizability of 5.35 $Å^3$ from the *Handbook of Chemistry and Physics*, 88th ed., edited by D. R. Lide (CRC, Boca Raton, FL, 2007), Sec. 10, p. 198, and a dipole moment of 1.8963 D from Sec. 9, p. 50. For NF_3 we used a polarizability of 3.62 $Å^3$ from Sec. 10, p. 197 and a dipole moment of 0.235 D from Sec. 9, p. 48.

[33] T. M. Miller, J. F. Friedman, A. E. S. Miller, and J. F. Paulson, J. Phys. Chem. **98**, 6144 (1994).

[34] D. Smith, N. G. Adams, and E. Alge, J. Phys. B **17**, 461 (1984).

[35] T. M. Miller, J. F. Friedman, A. E. S. Miller, and J. F. Paulson, Int. J. Mass Spectrom. Ion Process. **149–150**, 111 (1995).

[36] T. M. Miller, J. F. Friedman, and A. A. Viggiano, J. Chem. Phys. **120**, 7024 (2004). There is a misprint in Table II of this paper: the C–F bond lengths in c-C4F8 are all 1.410 Å for the G3(MP2) method, which uses a MP2(Full)/6–31G(d) geometry optimization. Also, the typical concentration of c-C4F8 vapor in the flow tube was misstated; it should read 4 ppmv.

[37] L. A. Curtiss, K. Raghavachari, P. C. Redfern, V. Rassolov, and J. A. Pople, J. Chem. Phys. **109**, 7754 (1998); L. A. Curtiss, P. C. Redfern, and K. Raghavachari, *ibid.* **123**, 124107 (2005).

[38] GAUSSIAN-03W, Revision C.02, M. J. Frisch, G. W. Trucks, H. B. Schlegel, G. E. Scuseria, M. A. Robb, J. R. Cheeseman, J. A. Montgomery, Jr., T. Vreven, K. N. Kudin, J. C. Burant, J. M. Millam, S. S. Iyengar, J. Tomasi, V. Barone, B. Mennucci, M. Cossi, G. Scalmani, N. Rega, G. A. Petersson, H. Nakatsuji, M. Hada, M. Ehara, K. Toyota, R. Fukuda, J. Hasegawa, M. Ishida, T. Nakajima, Y. Honda, O. Kitao, H. Nakai, M. Klene, X. Li, J. E. Knox, H. P. Hratchian, J. B. Cross, V. Bakken, C. Adamo, J. Jaramillo, R. Gomperts, R. E. Stratmann, O. Yazyev, A. J. Austin, R. Cammi, C. Pomelli, J. W. Ochterski, P. Y. Ayala, K. Morokuma, G. A. Voth, P. Salvador, J. J. Dannenberg, V. G. Zakrzewski, S. Dapprich, A. D. Daniels, M. C. Strain, O. Farkas, D. K. Malick, A. D. Rabuck, K. Raghavachari, J. B. Foresman, J. V. Ortiz, Q. Cui, A. G. Baboul, S. Clifford, J. Cioslowski, B. B. Stefanov, G. Liu, A. Liashenko, P. Piskorz, I. Komaromi, R. L. Martin, D. J. Fox, T. Keith, M. A. Al-Laham, C. Y. Peng, A. Nanayakkara, M. Challacombe, P. M. W. Gill, B. Johnson, W. Chen, M. W. Wong, C. Gonzalez, and J. A. Pople, Gaussian, Inc., Wallingford CT, 2004.

[39] N. Ruckhaberle, L. Lehmann, S. Matejcik, E. Illenberger, Y. Bouteiller, V. Periquet, L. Museur, C. Desfrancüois, and J.-P. Schermann, J. Phys. Chem. A **101**, 9942 (1997).

[40] C. Blondel, C. Delsart, and F. Goldfarb, J. Phys. B **34**, L281 (2001).

[41] U. Berzinsh, M. Gustafsson, D. Hanstorp, A. E. Klinkmueller, U. Ljunghlad, and A.-M. Maartensson-Pendrill, Phys. Rev. A **51**, 231 (1995).

[42] G. B. Ellison, P. C. Engelking, and W. C. Lineberger, J. Am. Chem. Soc. **100**, 2556 (1978).

[43] E. I. Dashevskaya, I. Litvin, E. E. Nikitin, and J. Troe, Phys. Chem. Chem. Phys. **10**, 1270 (2008). In evaluating collisional rate constants for NF_3 and CH_3Cl, we used the molecular properties listed in the citation of Ref. 32 above.

[44] I. I. Fabrikant and H. Hotop, J. Chem. Phys. **128**, 124308 (2008).

[45] M. W. Chase, J. Phys. Chem. Ref. Data Monogr. **9**, 1 (1998); We accessed these data on the Internet, at http://WebBook.NIST.gov/.

[46] R. S. Wilde, G. A. Gallup, and I. I. Fabrikant, J. Phys. B **33**, 5479 (2000).

[47] Z. Lj. Petrovic, W. C. Wang, and L. C. Lee, J. Chem. Phys. **90**, 3145 (1989).

[48] T. Ko, A. Fontijn, K. P. Lim, and J. V. Michael, Proceedings of the 24th Symposium (International) on Combustion, (The Combustion Institute, Pittsburgh, 1992), p. 735.

[49] N. C. Jones, D. Field, and J.-P. Ziesel, Int. J. Mass Spectrom. **277**, 91 (2008).

[50] D. M. Pearl, P. D. Burrow, I. I. Fahrikant, and G. A. Gallup, J. Chem. Phys. **102**, 2737 (1995).

[51] P. G. Datskos, L. G. Christophorou, and J. G. Carter, Chem. Phys. Lett. **168**, 324 (1990).

[52] I. I. Fahrikant, J. Phys. B **27**, 4325 (1994).

[53] X. Shi, V. K. Chan, G. A. Gallup, and P. D. Burrow, J. Chem. Phys. **104**,

1855 (1996); X. Shi, T. M. Stephen, and P. D. Burrow, *ibid.* **96**, 4037 (1992).

[54] G. A. Gallup and I. I. Fabrikant, Phys. Rev. A **75**, 032719 (2007).

[55] A. Schramm, I. I. Fahrikant, J. M. Weher, E. Leber, M.-W. Ruf, and H. Hotop, J. Phys. B **32**, 2153 (1999).

[56] M. Braun, I. I. Fabrikant, M.-W. Ruf, and H. Hotop, J. Phys. B **40**, 659 (2007).

[57] K. Nagesha, I. I. Fabrikant, and L. Sanche, J. Chem. Phys. **114**, 4934 (2001).

[58] I. I. Fabrikant, Phys. Rev. A **76**, 012902 (2007).